A generic study of the safety aspects of LMFBR roof covers under HCDA load conditions

B.L. SMITH, J.F. JAEGER, H.U. WENGER, C. INVERSINI

Federal Institute for Reactor Research, Würenlingen, Switzerland

The response of an LMFBR roof cover to HCDA loadings is examined using a combined 2D/3D modelling approach. A generic 3D roof design of box-type construction is adopted and analysis under specimen loads carried out using the finite element program ADINA. The reactor tank and all internal components below roof level are assumed axisymmetric with the containment code SEURBNUK-EURDYN employed to follow the accident progression. An interface between SEURBNUK-EURDYN and ADINA is provided via a 2D simulant roof model, chosen to match the principal response characteristics of the 3D roof, to enable any interaction effects occurring during impact to be assessed.

INTRODUCTION

1. The roof of a pool-type LMFBR performs an essential component support function and, together with the main vessel, forms part of the primary containment closure. During an HCDA the roof structure is subjected to large forces and its mechanical response, with particular regard to the prevention of leakage of radioactive material to the environment, is an important component in the assessment of overall containment integrity. Of particular concern is the possibility of direct pressure loading on the roof as a result of the impact from below of an accelerated coolant slug.

2. Detailed analysis of roof response is best undertaken using an appropriate structural code with 3D capability. Finite element programs such as ADINA [1], MSC/NASTRAN [2], ABAQUS [3], preferably backed up by computed aided graphics software such as UNISTRUC [4], provide the modelling sophistication necessary for the task. In addition, a number of hydrodynamics codes have been developed [5] to estimate HCDA roof loads, and to help in the general assessment of containment strength below roof level. These codes are very complex, usually restricted to 2D axisymmetric geometry, and require extensive validation programmes [6] to ensure reliability.

3. Traditionally, roof loading and reponse analyses have been decoupled, a strategy strictly valid only if roof response times are long compared to the load times, but is otherwise adopted for convenience. Roof loads, via structural load paths and by direct coolant impact, are first estimated under rigid roof assumptions, and then detailed study of the roof response is undertaken independently.

4. However, the roof is a very massive structure and could absorb considerable energy during the period of the load transient, mitigating damage effects elsewhere in the containment. A generic study of the interaction effects is reported in this paper. A particular feature of the work is the interfacing between the 2D axisymmetric reactor description adopted below roof level and the 3D roof representation. This is provided via a 2D simulant roof model, chosen to match the non-linear response behaviour of the 3D roof, and enables any interaction effects occurring during loading to be assessed. The principal analysis tools adopted for the study are the structural code ADINA [1], for the 3D and 2D roof modelling, and the containment code SEURBNUK-EURDYN [7], to follow the fluid structure interactions.

3D ROOF MODEL

5. Since we aim to estimate the energy absorbing capacity of a typical LMFBR roof structure, and its influence on overall containment integrity, we adopt a roof model sufficiently realistic to be representative of current design thinking but at the same time avoiding, as far as possible, design specific details. The model chosen is shown in Figure 1.

6. The central plug is assumed stiff while the annular portion is a box like structure of plate steel made up of top and bottom facing plates, radial shear webs, inner and outer rings, and a cylindrical support skirt. A ring of steel-lined holes of equal radius is used to represent the major roof penetrations for the pumps and IHX's. All plates are of 50 mm thickness and modelled using triangular 3D plate elements from the ADINA library. The box is completely filled with concrete modelled as 4 layers of 8-cornered solid elements matching the steel mesh. Because of mirror symmetry, only a sector of the roof annulus is modelled explicitly.

7. The coupling between the central plug (which incorporates the various rotating shields) and the inner ring of the roof is assumed unable to withstand bending forces and a simple hinge connection is used. All other steel connections are stiff to simulate welds. The assumption is made that no shear forces are transferred between the steel plates and the concrete in-fill and that the steel can slide on the concrete surface but cannot separate from

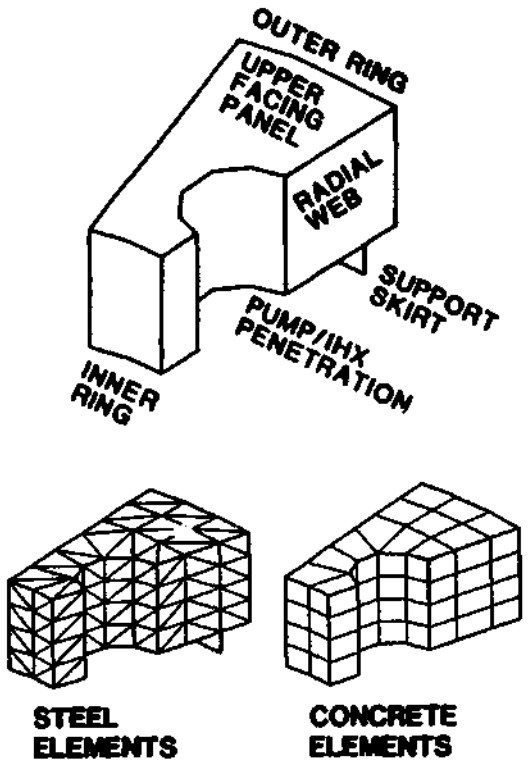

Figure 1 : ADINA Roof Model (3D)

it. The model is artificially stiffened by constraining some nodes to move together and spreading applied forces to avoid local stress concentrations which detailed design would eliminate. Further details of the model are given in References [8],[9].

2D REACTOR MODEL

8. A 2D axisymmetric representation is adopted for the reactor tank and for all internal components below roof level, Figure 2. Dimensions are appropriate for a commercial plant of 1300 MW(e) capacity.

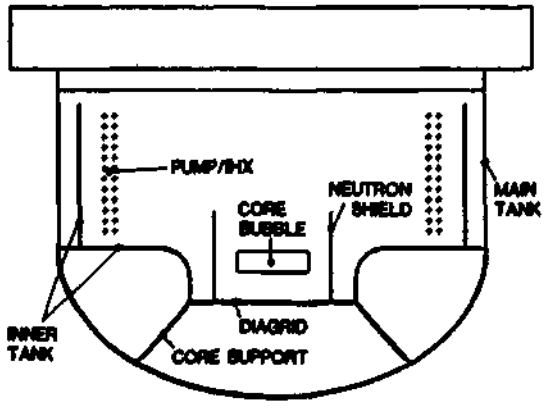

Figure 2 : Reactor Calculation (Rigid Roof)

9. The primary tank is cylindrical with a curved base and encloses the core and support structures, an inner tank separating the hot and cold sodium pools, as well as the pumps and IHX's. The core support assembly bears on the base of the main vessel to which it transmits loads resulting from the core pressurisation. The vessel in turn transmits the loads to the roof structure at its upper rim.

10. Many of the simplified structures seen in Figure 2 are composites of actual design features, and masses and strengths are enhanced accordingly. Thus, for example, the diagrid assembly includes a mass contribution arising from the core remnants, principally the radial and axial breeder zones. The neutron shield assembly has mass corresponding to the outer radial shield reflectors but strength compatible with a thin outer restraining barrel. The main tank has modified material properties to take account of the presence of nearby structures: the curved section above the junction with the diagrid support includes the mass and strength of the lower internal baffles, while the section below the junction incorporates the structural enhancement due to an attached core-catcher device.

11. The above core structure is assumed sufficiently weak for its effects on the flow dynamics to be ignored. The ring of IHX's and pumps, which experiments indicate do not produce strong asymmetries under HCDA conditions [10], is represented in a simplified way in which the blockage effect is taken into account by use of an annulus of porous material.

12. The energy source is provided by an expanding gas bubble of initial volume matching that of the inner fissile region of the core, and represents a work capacity of 1/2 GJ for an expansion to the cover gas volume.

13. In the finite element representation of the reactor model using SEURBNUK-EURDYN, all internal components are assembled using thin shell elements (not discernible in Figure 2). These may be generated automatically within the code and avoid unnecessary data preparation for those aspects of the problem not related directly to the calculation of the roof loads.

RIGID ROOF REACTOR CALCULATION

14. In the first instance we compute rigid roof loadings for input to the 3D ADINA roof model. Figure 3 shows the reactor configuration 115 msec into the transient, as calculated by SEURBNUK-EURDYN.

15. The bubble is seen to have expanded out of the core barrel, this having deformed considerably. The accelerated sodium slug above the bubble impacts the roof at 60 msec on the axis of symmetry. The impact zone spreads along the roof radius compressing the cover gas into the upper extremities of the vessel causing straining.

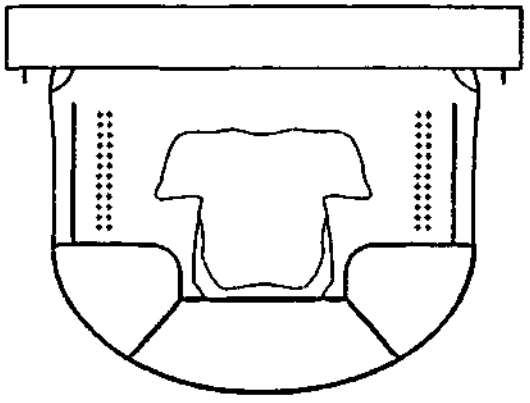

Figure 3 : Rigid Roof Calculation (t=115 msec)

16. The calculation was continued to 210 msec with the roof load histories given in Figure 4. At the start of the transient the core bubble pressure is high and the pressure differential across the diagrid is transmitted via connecting structures to produce a line load on the roof at the junction with the main tank; force 6 in Figure 4. This "pull-down" force peaks early at 6 MN/m due to plastic yielding of the tank. This value should be compared with the dead-weight load of 1 MN/m.

17. The second loading event occurs as a consequence of the slug impact, the roof loading being in the form of a pressure pulse of some 60 msec duration followed by a gradual pressurisation as the system approaches equilibrium. Pressures are displayed for five different radial locations in Figure 4. Peak pressures occur at progressively later times along the roof radius as the impact zone develops.

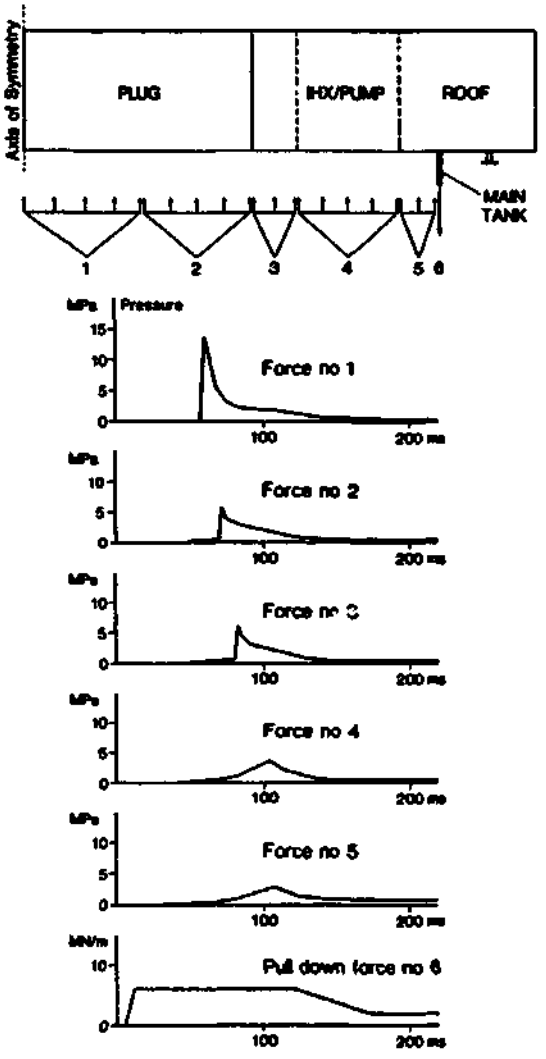

Figure 4 : Calculated Roof Loads

3D ROOF CALCULATION

18. The dynamic response of the 3D roof and plug assembly has been carried out using ADINA for the load functions given in Figure 4. The pull-down force transmitted by the main tank is applied across the roof thickness at the radius indicated in the Figure. The pressure distribution is assumed uniform at the five different areas of the bottom plate corresponding to the locations of the calculated slug pressure.

19. For the plug, which is not included in the finite element model, the resultant force is simulated by an appropriate line load applied to the inner ring of the roof annulus. Similar line loads have been used for the cylindrical area of the pump/IHX penetrations. Further details of the model are given in References [8],[9].

20. Both linear and non-linear analyses have been performed. In the non-linear regime the steel material response is assumed elastic-plastic with a yield criterion similar to von Mises, while ADINA's Drucker-Prager material model is used for the concrete with a tension cut-off and a cap on the compression strength, [8].

21. The results show that the roof structure is able to withstand the effects of the pull-down force within the linear range, but shortly after roof impact a wave of plasticity propagates from the inner ring along the vertical shear webs to the support skirt, Figure 5. There is some yielding of the top plate, indicated in the Figure, but the bottom plate remains unyielded throughout the loading period due to the high compression strength of the concrete above. Some non-linear behaviour for the concrete (cracking) is also observed.

22. For both the linear and non-linear cases very little lateral tipping of the model takes place (a few percents) and the global roof motion appears to be dominated by the fundamental radial mode.

2D EQUIVALENT ROOF MODEL

23. The absence of genuine 3D motions and the basic modal behaviour of the roof encourages us to look for a simple equivalent structure in the form of a homogeneous plate with modified material properties. For a plate of the correct

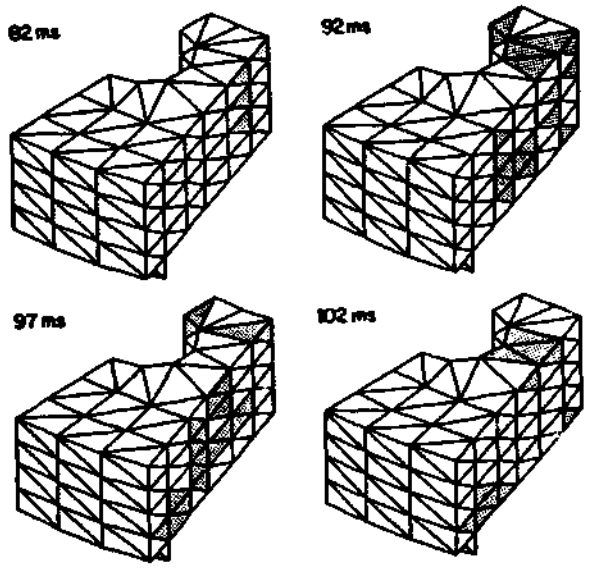

Figure 5 : Progress of Plasticity Wave

radial dimensions and of height h, the elastic lateral behaviour will be characterised by the two parameters ρh and Eh^3, representing inertia and flexural rigidity, respectively. The equivalent density ρ is chosen to preserve total mass while the equivalent Young's modulus E may be determined by matching static deflections or periods of free vibration. Fitting the vibration period proves to be more important as it will govern the whole time behaviour including the elastic recovery for the non-linear case. This will leave some error in the peak dynamic deflections.

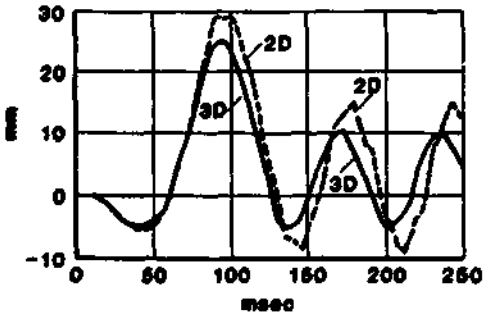

Figure 6 : Matching of Plug Displacements (Linear Model)

24. Plug displacement histories for the optimum linear 2D equivalence model are compared with those for the 3D model in Figure 6. In order to decouple the roof response from any effects due to the support skirt, the skirt was replaced by a simple support for these calculations. The load functions are those given in Figure 4 in both cases.

25. The initial dip in the plug deflection is due to the action of the pull-down force but the subsequent rise is accelerated by slug impact on the plug beginning at 60 msec. The period of free oscillation of the plug-roof assembly is 55 msec which is comparable to the pulse width of the loading function (see Figure 4). Results are given for a hinged coupling between the plug and the roof annulus, but the equivalence model proves to be sensibly independent of the coupling condition, [9]. The Young's modulus for the equivalent roof structure turns out to be very close to that used for the concrete in the 3D model indicative of the influence of the concrete stiffness on the total roof strength in the linear case.

26. When setting up the non-linear equivalence two further parameters become available: the yield strength σ_y of the material and the strain hardening slope E_1. The plug deflections for the 3D and 2D models are compared in Figure 7 for the best choice elastic/perfectly-plastic material (E_1=0); the yield strength σ_y being chosen to match the peak deflection.

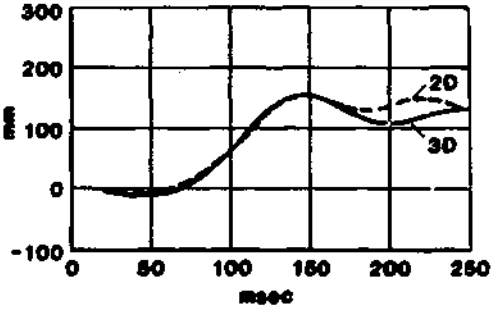

Figure 7 : Matching of Plug Displacements (Non-Linear Model)

27. The fit is not as close as in the linear case, particularly at later times, but there is no option to change the Young's modulus as the rise to the peak already occurs correctly. The final permanent offset however, is good. Note the factor 6 increase in peak deflection for the non-linear model.

28. The introduction of up to 4% strain hardening has very little effect on the results implying that the residual strength of the structure comes from the unyielded sections rather than work hardening effects elsewhere. The equivalence model in the non-linear case is more sensitive to the condition adopted for the plug-roof coupling than for the linear case. Full details are presented in Reference [9].

FLEXIBLE ROOF REACTOR CALCULATION

29. Refinement of the 2D equivalence model will mean a departure from the simple homogeneous plate to a more complex heterogeneous structure. In our case this is unnecessary since the divergence from the 3D results occurs after 170 msec (see Fig. 7) when the impact

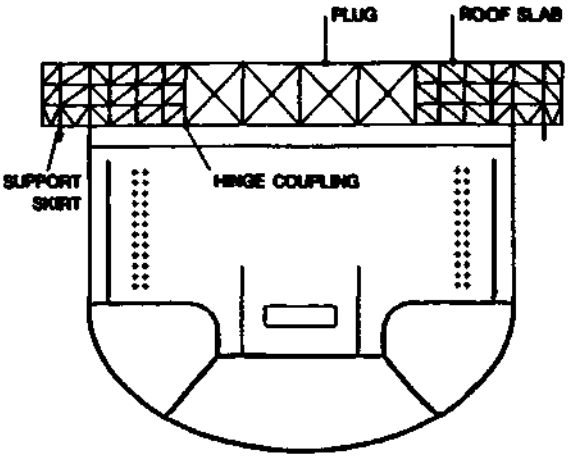

Figure 8 : Reactor Calculation (Flex Roof)

loading is complete. We can therefore examine the fluid-structure interaction effects occurring during the loading period using the existing model.

30. The flexible roof reactor configuration is given in Figure 8. Below roof level the arrangement is as before for the rigid roof case, but the roof and plug are now modelled explicitly using axisymmetric triangular elements from the EURDYN library, and the support skirt, made up of shell elements, is also included.

31. The SEURBNUK-EURDYN calculation was carried to 200 msec. The chronology of events before roof impact is almost identical with the rigid roof calculation. The downward displacement of the plug due to the action of the pull-down force peaks at about 40 msec and then there is partial elastic recovery before slug impact occurs at the plug centre at 60 msec. The high impact pressures further accelerate the roof assembly producing a peak plug displacement of 96 mm at t=160 msec. A sketch of the plug-roof coupling at maximum strain is given in Figure 9.

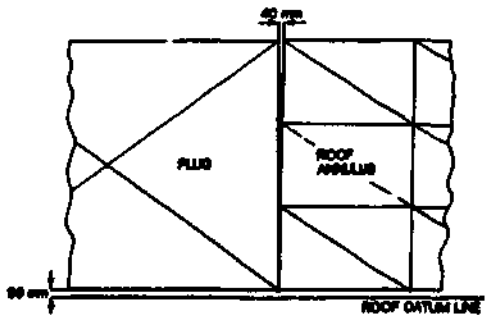

Figure 9 : Maximum Plug-Roof Separation

32. The principal post-loading event is the straining of the upper cylindrical portion of the main tank, occurring first near the junction with the roof but then spreading downwards. The reactor configuration at the final step in the calculation is shown in Figure 10 corresponding to a maximum bubble work of 550 MJ.

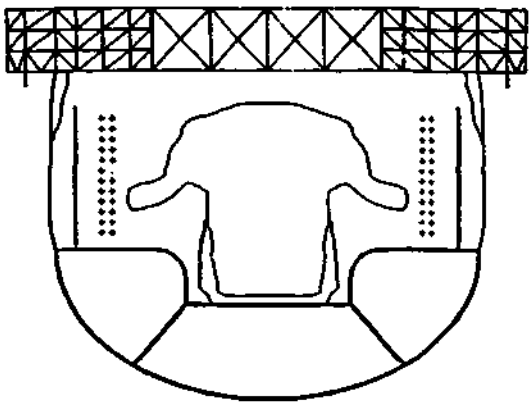

Figure 10 : Flex Roof Calculation (t=200 msec)

FINAL REMARKS

33. It has been shown that under the dynamic loads expected with HCDA phenomena it is possible, for the purposes of fluid-structure containment analyses, to represent the roof of a pool-type LMFBR with an axisymmetric model despite actual 3D design features due to penetrations, radial webs, the sandwiching of concrete in steel, and despite non-linear material behaviour. This is due to the lateral rigidity of the structure which limits azimuthal variations, and the dominance of the radial fundamental mode during loading. It has been demonstrated that a homogeneous plate with simple non-linear material properties is sufficient to match the principal response characteristics of the roof model adopted in this study. There appears to be little need for a more complex model.

34. Equivalent material properties are found by comparing 2D and 3D responses:
(1) Density is chosen to preserve mass;
(2) Young's modulus is adjusted to match the period of the linear responses, (the value found is close to that used for the concrete demonstrating the influence of the concrete stiffness on the linear motion);
(3) Material yield strength is chosen to match the amplitude of the non-linear response, (no strain hardening).

35. Concerning overall containment behaviour, the following observations can be made:
The roof model appears to be realistic, the maximum roof deflection (96 mm for a mechanical energy release of 550 MJ) calculated using the equivalent roof model, when appropriately scaled, agrees well with the deflection measured in the MARS experiment [11], a 1/20th scale mock-up test performed in France in support of the Superphenix safety analysis. The maximum

horizontal separation between the plug and roof upper surfaces, 40 mm in Figure 9, may have some consequences for some plug retention designs involving shear key arrangements. More detailed modelling of the plug-roof coupliug system is here indicated.

36. As remarked earlier, the transmission of the pull-down force to the roof early in the transient is limited by axial yielding of the main tank, which in our case has thickness 25 mm and is the only load bearing structure in contact with the roof, see Fig. 4. The transfer of the shear load to the support skirt, and hence to the reactor vault, via the radial web network is accomodated within the linear range of the steel. If however, there are additional load paths to the roof via inner tanks, baffles or pump shrouds, much larger forces may be transferred and the integrity of the roof structure under shear loads may need closer examination.

37. Due to the large strength and inertia of the plug-roof assembly, taking account of roof flexibility leads to only marginal reduction in the total roof load (2.5%) compared to the rigid roof case. This result implies that it is feasible to perform detailed structural analyses of the roof in isolation from the rest of the containment using rigid roof loadings:- the de-coupled approsch.

38. However, in the overall assessment of containment strength, and mechanical damage to structures below roof level, it is necessary to include the effects of roof flexibility. Figure 11 compares hoop strain histories for the cylindrical section of the main tank for the flexible and rigid roof calculations. The reduced final strain for the flexible roof case illustrates the significant energy absorbing capacity of the roof, even for modest roof displacements.

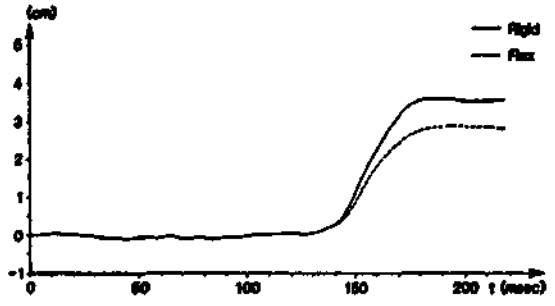

Figure 11 : Upper Vessel Hoop Strains

39. Thus results from the work completed so far show that in HCDA safety analyses detailed assessment of the strength of the roof structure can proceed adequately using rigid roof loads, but in the general assessment of containment integrity for weaker structures below roof level, account must be taken of the energy absorption due to roof movement in order to reduce conservatism.

REFERENCES

1. "ADINA - A Finite Element Program for Automatic Dynamic Incremental Nonlinear Analysis". ADINA Engineering Report AE 81-1, Watertown, MA (Sept. 1981).

2. McCORMICK,C.W. "MSC/NASTRAN - User's Manual" MacNeal-Schwendler Corp., California (1978).

3. HIBBITT,H.D. "ABAQUS/EPGEN - A General Purpose Finite Element Code with Emphasis on Non-Linear Applications", Nucl.Eng.Des., 77, 271 (1984).

4. UNISTRUC, Control Data Corporation, Minneapolis, Minnesota (1978).

5. CHANG,Y.W. "Analysis of HCDA", Nucl.Eng. Des., 69, 345 (1982).

6. ALBERTINI,C. et al "The JRC-COVA Programme, Final Report", EURATOM Report EUR 8705 EN (1983).

7. SMITH,B.L. "A New Fluid-Structure Coupling Algorithm for the LMFBR Containment Code SEURBNUK-EURDYN", Paper B2/6, SMIRT-8, Brussels (Aug 1985).

8. SAURER,G. et al "Dynamic Response of an LMFBR Deck Structure Under Slug Impact", Computers & Structures, 21, 159 (1985).

9. JAEGER,J.P. et al "Modelling of an LMFBR Cover for Fluid-Structure Interaction Studies", Paper E7/7, SMIRT-8, Brussels (Aug 1985).

10. BRASSINDALE,J.A. et al "Three Dimensional Aspects of Fast Reactor Containment Loading Studies", Paper E1/1, SMIRT-7, Chicago (Aug 1983).

11. PALGAYRETTES,M. et al "Response of a 1/20 Scale Mock-Up of the SUPER-PHENIX Breeder Reactor to an HCDA Loading Simulation", Paper E4/1, SMIRT-7, Chicago (Aug 1983).

The origin and magnitude of pressures in fuel coolant interactions

W. HEER, D. JAKEMAN, B.L. SMITH

Federal Institute for Reactor Research, Würenlingen, Switzerland

A number of small scale experiments to simulate fuel coolant interaction (FCI) effects have been carried out using Freon and water. Contrary to the predictions of most current FCI models, only modest pressure transients are observed within the interaction region itself but large pressure spikes, near to or above critical Freon pressure, are seen at the boundaries of the region. Similar pressure amplification effects have been noticed in parallel experiments involving two phase mixtures. It is suggested that in both cases a water hammer type effect is the cause of the pressure spikes. These observations could form the basis of new thinking in FCI modelling.

INTRODUCTION

1. In spite of the attention paid to fuel coolant interactions (FCI's) and the consequences of them in fast reactor safety philosophy, the underlying physical principles of the interaction are still not fully inderstood. An examination of some aspects of the problem has been carried out in simple geometries in the context of a number of small scale experiments. Particular attention is paid to the origin of high pressures commonly associated with FCI's.

INTERACTIONS WITH FREON AND WATER

2. To study the behaviour of FCIs, Freon, simulating the coolant, is poured into a narrow tube partially filled with water at 80 °C simulating the molten fuel. The type of Freon used is $ClCHF_2$ (boiling point: -40.8 °C, crit. temperature: 96 °C, crit. pressure: 4.9 MPa). A square aluminium tube (inner width: 3 cm) is used but square Perspex tubes are also employed to give an additional visual display. Pressure transients are measured at various locations along the length of the tube by piezo-electric pressure transducers (Kistler 6031 or 603B) and recorded by a 12 channel memory transient recorder. To facilitate interpretation, flash photographs are taken and, for selected tests, high speed cine photography (5000 f/s) is also used.

3. Out of 110 tests carried out 91 tests produced a significant interaction. Common to all tests is the appearance of a quasi-stable premixing zone of several cm length at the upper end of the water column. The zone remains in a churning state for about ½ s before the interaction spontaneously starts and rapidly spreads over the entire premixing zone. Although every test shows individual features in its pressure trace there is nevertheless surprisingly good consistency between groups of tests selected according to where the interaction started. Two types may be identified, those in which the interaction started near the bottom of the interaction region (type 1) and those in which the interaction started near the top (type 2). Fig. 1 shows a typical set of pressure traces for each type. Some 17 % of the interactions were of type 1, 37 % of type 2. In the remaining tests the interactions started at an intermediate point, and in these cases type 1 behaviour was observed above the starting point and type 2 behaviour below. Type 1 interactions propagate upwards with an average velocity of 120±50 m/s (min. 60 m/s) and a pressure pulse of average size 0.7±0.2 MPa (min. 0.35 MPa, max. 1.0 MPa). Type 2 interactions, propagating downwards, have essentially the same behaviour within the interaction region itself (average velocity: 150±80 m/s, min. velocity: 50 m/s, average pressure 0.7±0.2 MPa) but as soon as the pressure waves reach the lowest transducer positions (< 60 mm) high pressure spikes up to 6 MPa are observed. Photographs taken at various times during the interaction indicate the passage of the wave front. Fig. 2 is a good example in which a type 2 interaction started near to pos.4 and had reached pos.2 when the flash lamp was triggered. The interaction propagates down to pos.1 where the large pressure spike is produced. The Figure shows also a reflected wave similar in amplitude and velocity to the initial wave and superimposed on it. This behaviour is associated with the bottom edge of the interaction region lying between pos.1 and 2. The Freon seen in the photograph below pos.1 did not react in this case. Below the interaction region the pressure spike is transmitted through the water and is itself reflected at the bottom of the tube. The separation of the downward and reflected peaks at pos.1 suggests a velocity of about 1000 m/s, well in excess of the propagation speeds within the interaction region above. The pressure traces further indicate that only 30 % of the peak heights at pos.1 are due to superposition.

4. The generation of pressure spikes can be explained in the following way. Pressure waves passing through the essentially two phase interaction region accelerate (and compress) the